THIN CURRENT SHEET FORMATION: COMPARISON BETWEEN EARTH'S MAGNETOTAIL AND CORONAL STREAMERS

Artemyev A. V., 1 Réville V., 2 Ivan Zimovets, 3 Nishimura Y., 4 Velli M., 1 Runov A., 1 and Angelopoulos V. 1

(Received May 5, 2022) Submitted to ApJ

ABSTRACT

Magnetic field line reconnection is a universal plasma process responsible for the magnetic field topology change and magnetic field energy dissipation into charged particle heating and acceleration. In many systems, the conditions leading to the magnetic reconnection are determined by the prereconnection configuration of a thin layer with intense currents – otherwise known as the thin current sheet. In this study we investigate two such systems: Earth's magnetotail and helmet streamers in the solar corona. The pre-reconnection current sheet evolution has been intensely studied in the magnetotail, where in-situ spacecraft observations are available; but helmet streamer current sheets studies are fewer, due to lack of in-situ observations – they are mostly investigated with numerical simulations and information that can be surmised from remote sensing instrumentation. Both systems exhibit qualitatively the same behavior, despite their largely different Mach numbers, much higher at the solar corona than at the magnetotail. Comparison of spacecraft data (from the magnetotail) with numerical simulations (for helmet streamers) shows that the pre-reconnection current sheet thinning, for both cases, is primarily controlled by plasma pressure gradients. Scaling laws of the current density, magnetic field, and pressure gradients are the same for both systems. We discuss how magnetotail observations and kinetic simulations can be utilized to improve our understanding and modeling of the helmet streamer current sheets.

Keywords: solar wind – turbulence

Corresponding author: Anton V. Artemyev

aartemyev@igpp.ucla.edu

¹Department of Earth, Planetary, and Space Sciences and Institute of Geophysics and Planetary Physics, University of California, Los Angeles, California, USA

²IRAP, Université Toulouse III—Paul Sabatier, CNRS, CNES, Toulouse, France

³Space Research Institute, RAS, Moscow, Russia

⁴Department of Electrical and Computer Engineering and Center for Space Sciences, Boston University, Boston, MA USA

1. INTRODUCTION

Magnetic field-line reconnection is a key plasma process responsible for energy transformation and charged particle acceleration in solar corona (see, e.g., Priest & Forbes 2002; Aschwanden 2002; Zharkova et al. 2011) and planetary magnetospheres (see, e.g., reviews by Jackman et al. 2014; Gonzalez & Parker 2016; Birn & Priest 2007). Spatially localized regions of intense plasma currents, i.e., current sheets, are believed to be the primary regions where magnetic reconnection takes place (Biskamp 2000; Parker 1994; Birn & Priest 2007). The spatial spatial structure (topology) of currents sheets in the solar corona (Priest 1985, 2016) is generally much more complex than that in planetary magnetospheres. However, one notable exception is the helmet streamer current sheet, which shares many similarities in configuration with the most-investigated magnetotail current sheet (see discussion Syrovatskii 1981; Terasawa et al. 2000; Reeves et al. 2008).

A zero order approximation of the current sheet configuration in both the magnetotail and helmet streamers is provided by the Grad-Shafranov equation $\nabla \times \nabla \times A = 4\pi j$, in which a single vector potential component A(x,z) determines the field and the current density j in the systems' 2D plane geometry (for the solar corona x refers to the radial distance r, and z is along the direction of solar colatitude). However, the two systems differ in that for the magnetotail j = -dP/dA is due to diamagnetic drifts of the hot plasma, that which contributes to pressure P (Schindler & Birn 1978; Birn et al. 1977), whereas for the helmet streamer j is altered by the gravitational force $F_G(r)$ and dynamical pressure gradients $\sim \mathbf{v}\nabla\mathbf{v}$ (Pneuman & Kopp 1971). Although such flows can be included into a generalized magnetotail current sheet equilibrium with incompressible plasma (Birn 1991, 1992), in the absence of conductivity such a generalization is possible only for field-aligned $\mathbf{v} \propto \mathbf{B} \sim$ $-\nabla A$ flows (see details in Nickeler & Wiegelmann 2010). Such currents (produced by gradients of thermal and dynamical pressures) stretch magnetic field lines away from the Earth/Sun and reduce the magnetic field fall-off with radial distance (e.g., Washimi et al. 1987; Wang & Bhattacharjee 1999). A common methodology for reconstructing such current sheet configurations is to first identify system symmetries corresponding to integrals (e.g., Yeh 1984; Birn 1992; Hodgson & Neukirch 2015), which enables the derivations of the generalized Grad-Shafranov equation (see examples in Neukirch 1997, 1995a; Cheng 1992; Zaharia et al. 2005).

One additional important plasma property that needs to be incorporated in the equations describing helmet streamer current sheets, but is not typically considered in similar descriptions of the magnetotail, is temperature inhomogeneity due to the plasma thermal conductivity (Yeh & Pneuman 1977; Cuperman et al. 1990). The interplay of plasma temperature gradients and dynamical pressure gradients at different plasma beta, $\beta = 8\pi P/B^2$, significantly affects the evolution of helmet streamer current sheets (see Steinolfson et al. 1982). Cuperman et al. (1992, 1995) showed a significant difference of current sheet configurations modeled with polytropic pressure (typical equation of state for the magnetotail current sheet models) and with the pressure determined by the thermal conductance (typical equation of state for the Solar corona current sheet models).

The most advanced fluid models of magnetotail and helmet streamer current sheets describe 3D magnetic field configurations (e.g., Cuperman et al. 1993; Linker et al. 2001; Birn et al. 2004) or include a multi-fluid Hall physics (e.g., Endeve et al. 2004; Ofman et al. 2011, 2015; Rastätter et al. 1999; Yin & Winske 2002). However, kinetic physics, whereby the particle distribution functions and not just their moments are included in the dynamical evolution of the system, cannot be incorporated in system-scale models. Such physics is mostly investigated and validated in small-scale (spatially

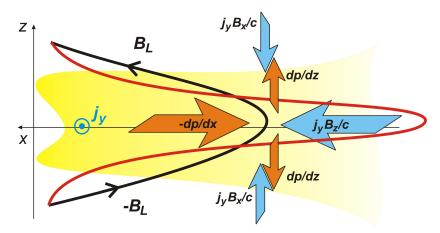


Figure 1. Schematic view of the magnetotail current sheet thinning with the main physical characteristics indicated. Two magnetic field lines are shown: parabolic black line before thinning and stretched red line after thinning.

localized) simulations available and justified for the magnetotail (see Pritchett & Coroniti 1994, 1995; Birn & Hesse 2005; Birn & Hesse 2014; Liu et al. 2014).

Both the magnetotail and helmet streamer current sheets are primary regions of magnetic field-line reconnection that is driven externally in both systems (e.g., Guo et al. 1996; Guo & Wu 1998; Verneta et al. 1994; Airapetian et al. 2011; Birn et al. 1996, 2004). Thus, the construction of accurate current sheet configurations is important to set realistic initial conditions for dynamical simulations of the magnetic reconnection and plasma heating (see discussion in Wu & Guo 1997a,b). A slow current sheet evolution, i.e., the current sheet thinning (e.g., Wiegelmann & Schindler 1995; Birn et al. 1998), plays a crucial role in determining the pre-reconnection current sheet configuration, which further controls the efficiency of the magnetic field energy dissipation and plasma heating. There is a good similarity in theoretical approaches for construction of such current sheet configurations (see discussion in Schindler et al. 1983; Neukirch 1997) and investigation of the current sheet stability (see discussion in Birn & Hesse 2009). An open question here is whether plasma flows play more important roles for the stability of the coronal current sheets (see, e.g., Dahlburg & Karpen 1995; Einaudi 1999; Lapenta & Knoll 2003; Feng et al. 2013) than for the magnetotail current sheet stability (see discussion in Shi et al. 2021). In hot magnetotail plasma, such flows may drive a slow current sheet evolution (see discussion in Nishimura & Lyons 2016; Pritchett & Lu 2018), but cannot determine the current sheet configuration, whereas in the corona plasma flows may contribute to the current sheet configuration (see discussion in Pneuman & Kopp 1971; Neukirch 1995b).

Magnetic field configuration of helmet streamer current sheets are observed in-situ only at large distances from the current sheet formation region (see, e.g., discussion in Pneuman 1972; Gosling et al. 1981; Eselevich & Filippov 1988; Bavassano et al. 1997), and mostly probed remotely (e.g., Woo 1997; Gopalswamy 2003). However, reconnection-related plasma injections from helmet streamer current sheets can be well captured (see most recent results in Korreck et al. 2020; Nieves-Chinchilla et al. 2020; Lee et al. 2021; Liewer et al. 2021, and references therein), which underlines the importance of investigating the reconnection and pre-reconnection dynamics of helmet streamer current sheets. In contrast to helmet streamer current sheets, the configuration of the magnetotail current sheet is well studied with multiple in-situ plasma and magnetic field measurements (see reviews by Baumjohann

et al. 2007; Artemyev & Zelenyi 2013; Petrukovich et al. 2015; Sitnov et al. 2019, and references therein). Therefore, observational aspects of the magnetotail current sheet thinning (formation of the thin current sheet before reconnection onset, see Runov et al. (2021a) and references therein) can be compared with models of helmet streamer current sheets.

In this study we focus on such a comparison of magnetotail current sheet observations and helmet streamer current sheet simulations, especially during the current sheet thinning. In the magnetotail current sheet configuration, such slow thinning can be treated as a 2D process with a fine balance between the magnetic field line tension and plasma pressure gradient (see schematic 1). To simulate the same current sheet thinning in the helmet streamer, we use a fluid model (see details in Réville et al. 2020a,b) based on PLUTO code (Mignone et al. 2007). We compare temporal profiles of stress balance components, magnetic field and current density magnitudes for the two systems and show similarities of the thin current sheet formation.

The paper is structured as follows: Sections 2.1 and 2.2 describe the basic spacecraft datasets for the magnetotail current sheet and the simulation setup for the helmet streamer; Section 3 compares stress balance dynamics in current sheet thinning for two systems, and Section 4 discusses main results.

2. SPACECRAFT OBSERVATIONS AND SIMULATION DATASETS

2.1. Magnetotail observations

Spacecraft observations of the magnetotail current sheet thinning before the reconnection onset form the basement for the magnetosphere substorm concept (see Baker et al. 1996; Angelopoulos et al. 2008a, and references therein). One of the key elements of such thinning is the current density j_u increase (see geometrical schematic in Fig. 1), which can be only reliably measured by multi-spacecraft with the curlometer technique (Dunlop et al. 2002; Runov et al. 2005). Therefore, statistical investigations of the current sheet thinning start with the Cluster mission (Escoubet et al. 2001) having four spacecraft that can probe magnetic fields and magnetic field gradients (currents and current sheet thickness) in the thinning current sheet (see Kivelson et al. 2005; Petrukovich et al. 2007, 2013; Snekvik et al. 2012). However, due to their polar orbit, Cluster spacecraft did not spend long intervals in the slowly thinning current sheet, which are better probed by the THEMIS mission (Angelopoulos 2008) on equatorial orbits. Three THEMIS spacecraft may be in the same azimuthal y plane and locate above $(B_x > 0)$, below $(B_x < 0)$, and around $(B_x \sim 0)$ the current sheet neutral plane, the plane of the main magnetic field (B_x) reversal. Thus, gradients $\partial B_x/\partial z$, $\partial B_z/\partial z$ contributing to the current density j_y (see Fig. 1) can be calculated from the differences of magnetic field at three spacecraft (see Artemyev et al. 2016). Magnetic field B_x is a good proxy of the spacecraft distance relative to the neutral plane (where $B_x = 0$) and plasmasphere lobes (where B_x reaches maxima of B_L). In the magnetotail current sheet configuration $\partial B_x/\partial z \gg \partial B_z/\partial z$, and the lobe field B_L can be estimated from the pressure balance $\langle B_x^2 + 8\pi P \rangle = B_L^2$, where P is the plasma (ion and electron) pressure and $\langle \dots \rangle$ is the average over the interval of the current sheet crossing (see discussion of how B_L is reliable in Petrukovich et al. 1999).

Figure 2 (a) shows an example THEMIS observation of magnetic fields in the thinning current sheet. Magnetic field is measured by THEMIS fluxgate magnetometer (Auster et al. 2008) and normalized to B_L , which is calculated with plasma measurements from electrostatic analyzer (for energies below 30keV, see McFadden et al. 2008) and solid state detector (for energies between 30 and 500 keV,

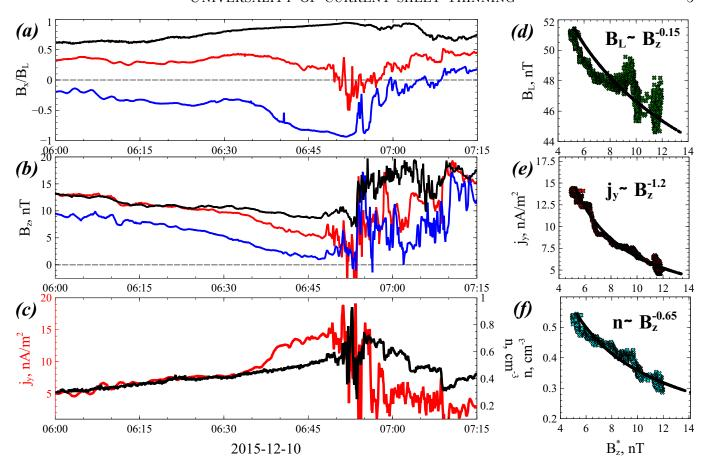


Figure 2. Example observations of the magnetotail current sheet thinning (before 06:50 UT) and thin current sheet destruction by plasma flows from the reconnection site (at 06:50 UT). Panels (a) and (b) show B_x and B_z magnetic field components measured by THEMIS A (black), D (red), and E (blue). Magnetic field B_x is normalized to the lobe magnetic field $B_L = \max |B_x|$ estimated from the pressure balance and plasma pressure measurements. Panel (c) shows current density $j_y = (c/4\pi) \cdot (\partial B_x/\partial z - \partial B_z/\partial x)$ and plasma density (measured by THEMIS D). Panels (d,e,f) show B_L , j_y , and n as a function of B_z^* (B_z^* is the B_z measured by the THEMIS spacecraft closest to the neutral plane) during the current sheet thinning. We also show fits of $B_L(B_z^*)$, $j_y(B_z^*)$, $n(B_z^*)$ by power law functions.

see Angelopoulos et al. 2008b). THEMIS D (red) is located close to the neutral sheet and observe B_x/B_L oscillations around zero, whereas THEMIS E (blue) and A (black) are located below and above the neutral plane and observe $|B_x/B_L|$ increases (the typical signature of the current sheet thinning) and $j_y \sim \Delta B_x$ growth. Simultaneous with B_x/B_L variations, all three THEMIS probes observe B_z decreases (see panel (b)), i.e., the current sheet thinning is accompanied by magnetic field line stretching (see discussion in Petrukovich et al. 2007). Thinning ends at around 06:50 UT by the reconnection onset downtail (at large radial distances). Plasma flows propagating from the reconnection site bring strong B_z increases (so-called dipolarization fronts (see Nakamura et al. 2002, 2009; Runov et al. 2009; Sitnov et al. 2009) that lead to B_x/B_z ratios close to the nominal dipole, $B_x/B_z \sim 1$) and destroy the thin current sheet (see $|B_x/B_L|$ decreases at THEMIS E and A).

The current sheet thinning and following destruction of thin current sheet can also be seen in the temporal profile of the current density j_y shown in panel (c). Before 06:50 UT, j_y goes up,

but then quickly drops to zero after the thin current sheet is destroyed by the dipolarization front. The current density increase is accompanied by plasma density increase, i.e., thinning current sheet becomes denser (see panel (c)). Statistical observations of the magnetotail current sheet thinning show that this density increase is due to the arrival of new cold plasma populations from deep magnetotail or ionosphere (e.g., Artemyev et al. 2019), and such a density increase is associated with a plasma temperature decrease (see Artemyev et al. 2016; Yushkov et al. 2021). Plasma cooling in the thinning current sheet contradicts to the concept of the compressional thinning (see Schindler & Birn 1986, 1999), and indeed the current density increase j_y is much stronger than B_L increase in thinning current sheets (see Artemyev et al. 2016; Sun et al. 2017). Thus, the formation of thin current sheet may mostly involve the interval reconfiguration of the current sheet with only a weak external driver.

As the equatorial magnetic field B_z monotonically decreases during the current sheet thinning, we can use it, instead of time, to trace the evolution of the current sheet configuration. Figure 2 (d,e,f) shows $B_L(B_z^*)$, $j_y(B_z^*)$, and $n(B_z^*)$ profiles for the interval with B_z^* decrease (B_z^* is the B_z measured by the THEMIS spacecraft closest to the neutral plane). The current density magnitude grows almost linearly with $1/B_z^*$; this means that the magnetic field line tension force $j_y B_z$, which balances the plasma pressure gradient at the equator $\partial P/\partial x$, does not vary much during the current sheet thinning. The lobe magnetic field (or equatorial plasma pressure $\approx B_L^2/8\pi$) varies with B_z slowly, and thus we indeed deal with the current sheet thinning: the current sheet thickness $L \approx c B_L/4\pi j_y \propto B_z$ goes down. The plasma density increases much faster then B_L^2 , and this confirms the plasma temperature decrease $T = P/n = B_L^2/8\pi n \propto B_z^{1/3}$.

Although the B_z decrease and j_y increase are characteristic features of the magnetotail current sheet thinning, rates of these processes may vary from event to event. Figure 3 shows statistical THEMIS observations of the current sheet thinning (Artemyev et al. 2016, for the database details ee). The current density variation is generally slightly faster than $\propto 1/B_z$, whereas the lobe field B_L increases generally slower than $\propto 1/B_z^{1/2}$, and this difference means that the j_y increase is accompanied by the current density decrease. Moreover, for many events B_L does not change $(B_L \propto 1/B_z^{1/4})$, indicating that the thin current sheet with intense j_y is growing inside a thicker plasma sheet supporting B_L , i.e., we deal with the so-called embedded current sheets (see Runov et al. 2006; Artemyev et al. 2010; Petrukovich et al. 2009). The typical thickness of an embedded thin current sheet is the proton gyroradius $\rho_p = \sqrt{m_p c^2 T_p}/eB_0$, as determined by the field B_0 at the boundary of the thin current sheet, $L \approx cB_0/4\pi j_y \approx \rho_p$ (Artemyev et al. 2011; Petrukovich et al. 2015). Although for most intense current sheets B_0 may reach B_L , i.e., the thin current sheet contains the entire cross-sheet current density, it is more usual to have $B_0 \sim B_L/3$ (Artemyev et al. 2010).

The plasma density increase is quite typical for the current sheet thinning (see left panel in Fig. 3), but the rate of this increase is smaller than the j_y increase rate. Thus, the total bulk speed of the current carriers (difference between ion and electron drifts) is growing, as $j_y/en \propto 1/B_z^{1/2}$, in the thinning current sheet.

In this work, we will compare observational trends of j_y , n, and plasma pressure $B_L^2/8\pi$ evolutions with the results of fluid simulations of the current sheet thinning in the helmet streamer configuration. The main difference of these two systems, magnetotail and helmet streamer, is the strong plasma flows absent in the pre-reconnection magnetotail, but potentially contributing to the helmet streamer current sheet configuration.

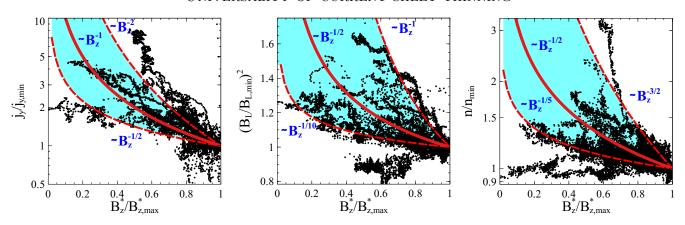


Figure 3. Statistical characteristics of current density, plasma density, and magnetic field magnitude evolution in thinning current sheets (B_z decreases with time). For each event from (Artemyev et al. 2016), we normalize the current density, lobe field, and plasma density to their nominally minimum values (the initial moment of time when spacecraft enter the thinning current sheet).

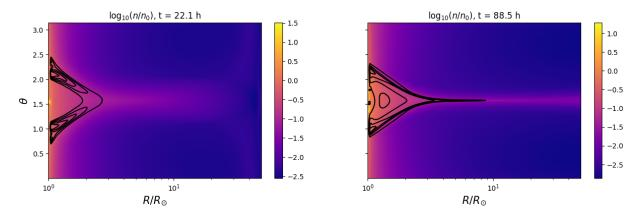


Figure 4. 2D view of the thin current sheet formation in helmet streamer geometry. For two moments of time we show $j_{\varphi} = const$ contours (black) and plasma density (color). The first moment (left) is the initial state and the final moment (right) is the current sheet right before the reconnection onset. The normalization factor for the plasma density is $n_0 = 10^8 \text{cm}^{-3}$.

2.2. Streamers' simulations

To simulate the helmet streamer current sheet, we use a 2.5D MHD code that includes effects of wave pressure and turbulent heating (see details in Réville et al. 2020a,b) based on the PLUTO code (Mignone et al. 2007). The simulation shown here repeats one from Réville et al. (2020a), with Lundquist number $S=10^5$. The simulation is initialized with a dipole field, while mechanisms of coronal heating and wind acceleration act to thin the heliospheric current sheet located at $\theta=\pi/2$. After about 90h of simulation time, a tearing instability is triggered in the current sheet. In the following, we focus on the thinning process.

Figure 4 shows the plasma density distribution and current density contours in the (r, θ) plane for the initial and final moment of the simulation, right before the reconnection onset at $r \sim 5r_{\odot}$. The radial direction r is an analog of x coordinate in the magnetotail current sheet, and $r \cos \theta$ is an analog of z coordinate (here θ is colatitude). A thin current sheet clearly develops in the stretched

magnetic field lines along the streamer, and we aim to compare dynamic properties of this current sheet thinning with the magnetotail observational dataset. To simplify the comparison we will focus on the stress balance equations along the radial direction in the neutral plane $\theta = \pi/2$:

$$\rho \frac{\partial v_r}{\partial t} + \underbrace{\rho v_r \frac{\partial v_r}{\partial r} + \rho \frac{v_\theta}{r} \frac{\partial v_r}{\partial \theta} - \frac{v_\theta^2}{r}}_{n[(\mathbf{v}\nabla)\mathbf{v}]_r} + \underbrace{\frac{\partial P}{\partial r} + \frac{1}{8\pi} \frac{1}{r^2} \frac{\partial r^2 B_\theta^2}{\partial r}}_{\nabla (P+B^2/8\pi)_r} = \underbrace{-\frac{g\rho}{r^2} + \frac{B_\theta}{4\pi r} \frac{\partial B_r}{\partial \theta}}_{[(\mathbf{B}\nabla)\mathbf{B}]_r/4\pi - g\rho/r^2}$$
(1)

where v_r and v_θ are radial and azimuthal velocity components, g is the gravitational constant of the Sun, and $\rho = nm_p$. Equation (1) shows that for slow (adiabatic) current sheet thinning, three main stress balance terms should be in balance: gradients of dynamic pressure $n[(\mathbf{v}\nabla)\mathbf{v}]_r$, total pressure $\nabla(P+B^2/8\pi)$, and magnetic field line tension force $[(\mathbf{B}\nabla)\mathbf{B}]$ with the gravitation correction $-gn/r^2$. The analog of Eq. (1) in the magnetotail current sheet configuration can be written as

$$\rho \frac{\partial v_x}{\partial t} + \underbrace{\rho \left(v_x \frac{\partial v_x}{\partial x} + v_z \frac{\partial v_x}{\partial z} \right)}_{\rho[(\mathbf{v}\nabla)\mathbf{v}]_x} + \underbrace{\frac{\partial P}{\partial x} + \frac{1}{8\pi} \frac{\partial B_z^2}{\partial x}}_{\nabla (P + B^2/8\pi)_x \approx \nabla_x P} = \underbrace{\frac{B_z}{4\pi} \frac{\partial B_x}{\partial z}}_{[(\mathbf{B}\nabla)\mathbf{B}]_x/4\pi \approx j_y B_z/c}$$
(2)

In the hot magnetotail plasma $P \gg \rho v^2/2$, there is no contribution of plasma flows to the current sheet configurations before the reconnection onset (Rich et al. 1972). Note that $\nabla P \gg \rho(\mathbf{v}\nabla)\mathbf{v}$ does not work for complex quasi-1D current sheet configurations that include nongyrotropic pressure terms (see discussion in Steinhauer et al. 2008; Artemyev et al. 2021, and reference therein).

3. DISCUSSION OF THE FORCE BALANCE IN THINNING CURRENT SHEETS

Figure 5 shows cross-sheet profiles (along θ) of main current sheet characteristics (magnetic field B_{θ} , plasma pressure P, and current density j_{φ}) and main terms of the stress balance (dynamical pressure, total pressure, and magnetic field line tension force) at different times of the simulation. Initially, θ profiles show the single scale, and the stress balance is provided by $\nabla(P + B^2/8\pi) \approx [(\mathbf{B}\nabla)\mathbf{B}]/4\pi$. Note that profiles in Fig. 5 are plotted at the radial distance where the magnetic reconnection will occur after ~ 18 h of simulation time.

The current sheet thinning is driven by a slight imbalance between the pressure gradient and the magnetic tension at the equator. As time goes on, a thin embedded current sheet develops in the central region of the simulation domain (see panel (b)). All three profiles of B_{θ} , P, and j_{φ} exhibit a gradient: strong peaks of j_{φ} and P (and minimum of B_{θ}) around the center region $(\theta = \pi/2)$, with almost unchanged levels (from the initial profile) elsewhere. The terms in the force balance equation also exhibit significantly different θ -profiles, but the current sheet is still balanced as $\nabla(P + B^2/8\pi) \approx [(\mathbf{B}\nabla)\mathbf{B}]/4\pi$, with secondary (small-scale) peaks of $(P + B^2/8\pi)$, $[(\mathbf{B}\nabla)\mathbf{B}]/4\pi$ around $\theta = \pi/2$.

Right before the reconnection onset (see panel (c)), the B_{θ} minimum at $\theta = \pi/2$ almost reaches zero, whereas the peaks in current density and plasma pressure become even stronger. The pressure peak is embedded in the initial large-scale profile. Similar peaks are formed in the force balance components, with the same balance provided by $\nabla(P + B^2/8\pi) \approx [(\mathbf{B}\nabla)\mathbf{B}]/4\pi$. There is a small minimum of $[(\mathbf{B}\nabla)\mathbf{B}]/4\pi$ at the center region $(\theta = \pi/2)$, which is likely balanced by the dynamic pressure gradient in the same region. However, magnitude of the dynamic pressure contribution to the stress balance remains small.

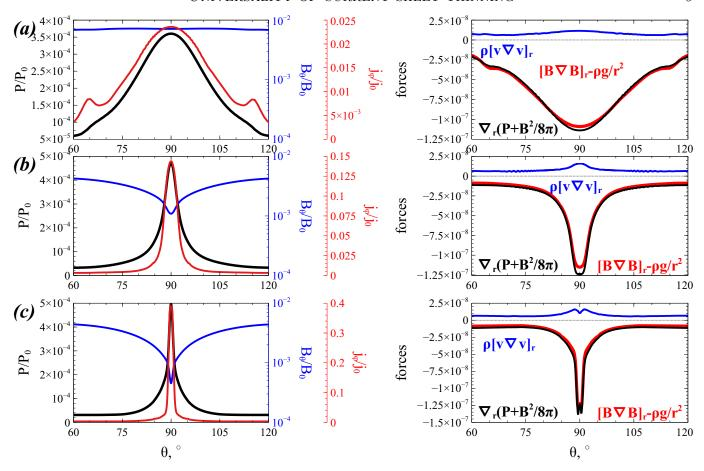


Figure 5. Left panels show cross-sheet θ-profiles of current density $j_{\varphi} = (r^{-1}\partial B_r/\partial\theta - \partial B_\theta/\partial r)$, normal magnetic field B_{θ} , and plasma pressure for three moments of time (t=0, t=5h, and t=18h). Right panels show cross-sheet θ-profiles of the three main terms of the radial stress balance. All profiles are plotted at the radial distance of the magnetic reconnection region, which occurs right after t=18h. Magnetic field components are normalized on $B_0 \approx 2$ Gauss, plasma pressure is normalized to $P_0 = 0.319$ dyne/cm², and the current density is normalized on $j_0 = cB_0/4\pi r_{\odot}$. All stress balance terms (forces) are in units of $kg/s^2/cm/r_{\odot}$.

Figure 6 shows the evolution of the main current sheet characteristics and stress balance terms at the current sheet center, $\theta = \pi/2$. There is a clear increase of the current density j_{φ} due to the formation of an embedded current sheet, which is accompanied by a decrease in B_{θ} . The balance between j_{φ} and B_{θ} variations results in an almost constant $j_{\varphi}B_{\theta} \approx [(\mathbf{B}\nabla)\mathbf{B}]_r$, which balances $\nabla(P+B^2/8\pi)_r$. Note that $\nabla(P+B^2/8\pi)_r$ does not vary because P only increases weakly. Therefore, the current sheet thinning also means the current sheet stretching with $L_r \approx P/(\nabla P)_r$ increasing proportionally to P. Note for the same magnetic field configuration, Réville et al. (2021) shows that the current sheet thinning is related to a pressure-driven instability, akin to the ballooning mode, whose timescales depend on the balance between magnetic curvature vector, gravity, and pressure gradients. Due to the stress balance along θ , the current sheet thickness can be estimated as $L \approx cB_0/j_{\varphi}4\pi$, with $B_0 \approx \sqrt{8\pi P}$. Thus, for the scale ratio we have $L_r/L \propto Pj_{\varphi}/B_0 \propto B_0/B_{\theta}$, where $j_{\varphi}B_{\theta} \sim const$. As $P \approx B_0^2/8\pi$ increases weakly and B_{θ} decreases, L_r/L increases during the current sheet thinning,

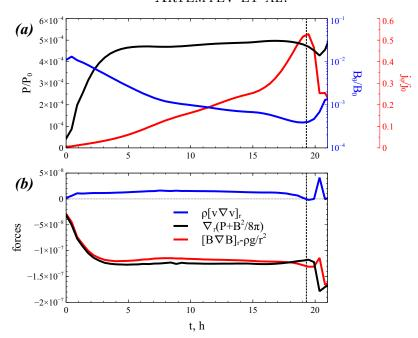


Figure 6. Evolution of the main current sheet characteristics and stress balance terms in the current sheet center, $\theta = \pi/2$. See details of the normalizations and units in the caption of Fig. 5.

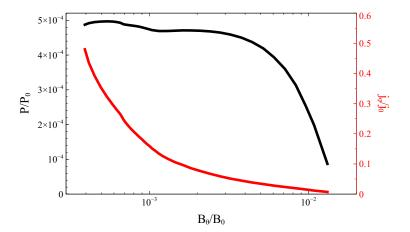


Figure 7. Profiles of the current density and plasma pressure from Fig. 6 plotted as a function of B_{θ} . See details of the normalizations and units in the caption of Fig. 5.

i.e., magnetic field lines stretching makes the current sheet more 1D (see also Fig. 4). This resembles the evolution of the magnetotail current sheet, where L_x/L also goes down during the current sheet thinning (see discussion in Petrukovich et al. 2013; Artemyev et al. 2016).

Similar to Fig. 2(d,e), Figure 7 shows j_{φ} , P as a function of B_{θ} . Figures 7, 3 show an important similarity of the thin current sheet formation in the helmet streamer system and in the Earth's magnetotail. In both systems the strong increase of the current density is not associated with the strong plasma pressure increase (equatorial $P \approx B_L^2/8\pi$ in the magnetotail), i.e., the current sheet thinning is characterized by an internal reconfiguration of the cross-sheet θ -profiles (z-profiles) of plasma pressure without significant loading of magnetic fluxes in current sheet boundaries. Therefore,

the pre-reconnection thin current sheet configuration in the helmet streamer, and the corresponding reconnection properties of this current sheet, are controlled by the internal nonlinear plasma dynamics rather than by external (boundary) variations. The same conclusion for the magnetotail has been acknowledged in series of models, which show the thin current sheet develops as a result of internal reconfiguration of the plasma and magnetic field, without strong variations of the magnetic field pressure in current sheet boundaries (see Birn et al. 1996, 2004; Hsieh & Otto 2015).

4. CONCLUSIONS

In this study we compare details of the thin current sheet formation in Earth's magnetotail (as derived from in-situ spacecraft observations) and in the helmet streamer magnetic field configuration (as derived from the MHD simulation). This comparison reveals interesting similarities of the current sheet thinning in both systems:

- Despite the different relation between thermal plasma pressure P and dynamic pressure $\rho v^2/2$ for the magnetotail $(P \gg \rho v^2/2)$ and helmet streamer configuration $(P \ll \rho v^2/2)$, in both systems the current sheet thinning is controlled by the fine balance of the magnetic field line tension force $\sim [(\mathbf{B}\nabla)\mathbf{B}]$ and plasma pressure gradient $\sim \nabla P$ around the narrow, near-equatorial layer of strong current density. Before the reconnection onset the dynamic plasma pressure contribution to the current sheet stress balance is not important.
- The current sheet thinning is associated with the current density increase and equatorial magnetic field decrease (keeping $j_{\varphi}B_{\theta}\approx const$), such that the magnetic field line tension force does not change much. Thus, there is no significant increase of the plasma pressure magnitude, and the thin current sheet formation is characterized by the internal reconfiguration of the current density and plasma pressure along z.

Similarities of these two systems suggest that many kinetic effects (Hall fields, collisionless conductivity, electron anisotropy, and ion nongyrotropy), typical for the thin magnetotail current sheet (see discussion in reviews by Artemyev & Zelenyi 2013; Sitnov et al. 2019; Runov et al. 2021a), may be valid for the thin current sheet formation in the helmet streamer configuration. Inclusion of such effects for large-scale systems as helmet streamers cannot be performed in full particle-in-cell simulations. However, some of these effects can be well reproduced in global hybrid simulations (see Lin et al. 2017; Lu et al. 2016, 2017, 2019), which cover spatial scales of planetary magnetospheres (e.g., Lin et al. 2014; Runov et al. 2021b), and may be applied to spatial scales of the helmet streamer systems.

ACKNOWLEDGEMENTS

This work is supported NASA DRIVE SCIENCE CENTER HERMES grant No. 80NSSC20K0604 (A.A., V.R., A.R., Y.N., M.V.) and by ERC SLOW SOURCE DLV-819189 (V.R.). I.Z. acknowledges the support from the Russian Science Foundation grant No. 17-72-20134, Y.N. was supported by NASA grant 80NSSC18K0657 and 80NSSC21K1321, NSF grant AGS-1907698 and AGS-2100975, and the "Magnetotail Dipolarizations: Archimedes Force or Ideal Collapse?" ISSI team.

We acknowledge NASA contract NAS5-02099 for use of THEMIS data. We would like to thank C. W. Carlson and J. P. McFadden for use of ESA data, D.E. Larson and R.P. Lin for use of SST data, K. H. Glassmeier, U. Auster, and W. Baumjohann for the use of FGM data provided under the

lead of the Technical University of Braunschweig and with a financial support through the German Ministry for Economy and Technology and the German Aerospace Center (DLR) under contract 50 OC 0302. THEMIS data were downloaded from http://themis.ssl.berkeley.edu/. Data access and processing was done using SPEDAS V4.1, see Angelopoulos et al. (2019).

REFERENCES

- Airapetian, V., Ofman, L., Sittler, E. C., & Kramar, M. 2011, ApJ, 728, 67, doi: 10.1088/0004-637X/728/1/67
- Angelopoulos, V. 2008, SSRv, 141, 5, doi: 10.1007/s11214-008-9336-1
- Angelopoulos, V., McFadden, J. P., Larson, D., et al. 2008a, Science, 321, 931, doi: 10.1126/science.1160495
- Angelopoulos, V., Sibeck, D., Carlson, C. W., et al. 2008b, SSRv, 141, 453, doi: 10.1007/s11214-008-9378-4
- Angelopoulos, V., Cruce, P., Drozdov, A., et al. 2019, SSRv, 215, 9, doi: 10.1007/s11214-018-0576-4
- Artemyev, A. V., Angelopoulos, V., Runov, A., & Petrukovich, A. A. 2016, J. Geophys. Res., 121, 6718, doi: 10.1002/2016JA022779
- 2019, Journal of Geophysical Research (Space Physics), 124, 264, doi: 10.1029/2018JA026113
- Artemyev, A. V., Petrukovich, A. A., Nakamura,
 R., & Zelenyi, L. M. 2010, J. Geophys. Res.,
 115, A12255, doi: 10.1029/2010JA015702
- —. 2011, J. Geophys. Res., 116, A0923, doi: 10.1029/2011JA016801
- Artemyev, A. V., & Zelenyi, L. M. 2013, Space Sci. Rev., 178, 419, doi: 10.1007/s11214-012-9954-5
- Artemyev, A. V., Lu, S., El-Alaoui, M., et al. 2021, Geophys. Res. Lett., 48, e92153, doi: 10.1029/2020GL092153
- Aschwanden, M. J. 2002, SSRv, 101, 1, doi: 10.1023/A:1019712124366
- Auster, H. U., Glassmeier, K. H., Magnes, W., et al. 2008, SSRv, 141, 235, doi: 10.1007/s11214-008-9365-9
- Baker, D. N., Pulkkinen, T. I., Angelopoulos, V.,Baumjohann, W., & McPherron, R. L. 1996,J. Geophys. Res., 101, 12975,doi: 10.1029/95JA03753
- Baumjohann, W., Roux, A., Le Contel, O., et al. 2007, Annales Geophysicae, 25, 1365

- Bavassano, B., Woo, R., & Bruno, R. 1997,Geophys. Res. Lett., 24, 1655,doi: 10.1029/97GL01630
- Birn, J. 1991, Physics of Fluids B, 3, 479, doi: 10.1063/1.859891
- —. 1992, J. Geophys. Res., 97, 16817, doi: 10.1029/92JA01527
- Birn, J., Dorelli, J. C., Hesse, M., & Schindler, K. 2004, J. Geophys. Res., 109, 2215, doi: 10.1029/2003JA010275
- Birn, J., & Hesse, M. 2005, Annales Geophysicae, 23, 3365, doi: 10.5194/angeo-23-3365-2005
- Birn, J., & Hesse, M. 2009, Annales Geophysicae, 27, 1067, doi: 10.5194/angeo-27-1067-2009
- —. 2014, J. Geophys. Res., 119, 290, doi: 10.1002/2013JA019354
- Birn, J., Hesse, M., & Schindler, K. 1996,J. Geophys. Res., 101, 12939,doi: 10.1029/96JA00611
- —. 1998, J. Geophys. Res., 103, 6843, doi: 10.1029/97JA03602
- Birn, J., & Priest, E. R. 2007, Reconnection of magnetic fields: magnetohydrodynamics and collisionless theory and observations, ed. Birn, J. & Priest, E. R.
- Birn, J., Sommer, R. R., & Schindler, K. 1977, J.Geophys. Res., 82, 147,doi: 10.1029/JA082i001p00147
- Biskamp, D. 2000, Magnetic Reconnection in Plasmas
- Cheng, C. Z. 1992, J. Geophys. Res., 97, 1497, doi: 10.1029/91JA02433
- Cuperman, S., Bruma, C., Detman, T., & Dryer,M. 1993, ApJ, 404, 356, doi: 10.1086/172285
- Cuperman, S., Bruma, C., Dryer, M., & Semel, M. 1995, A&A, 299, 389
- Cuperman, S., Detman, T. R., Bruma, C., & Dryer, M. 1992, A&A, 265, 785
- Cuperman, S., Ofman, L., & Dryer, M. 1990, ApJ, 350, 846, doi: 10.1086/168436

- Dahlburg, R. B., & Karpen, J. T. 1995,J. Geophys. Res., 100, 23489,doi: 10.1029/95JA02496
- Dunlop, M. W., Balogh, A., Glassmeier, K.-H., & Robert, P. 2002, J. Geophys. Res., 107, 1384, doi: 10.1029/2001JA005088
- Einaudi, G. 1999, Plasma Physics and Controlled Fusion, 41, A293, doi: 10.1088/0741-3335/41/3A/023
- Endeve, E., Holzer, T. E., & Leer, E. 2004, ApJ, 603, 307, doi: 10.1086/381239
- Escoubet, C. P., Fehringer, M., & Goldstein, M. 2001, Annales Geophysicae, 19, 1197, doi: 10.5194/angeo-19-1197-2001
- Eselevich, V. G., & Filippov, M. A. 1988, Planet. Space Sci., 36, 105, doi: 10.1016/0032-0633(88)90046-3
- Feng, L., Inhester, B., & Gan, W. Q. 2013, ApJ, 774, 141, doi: 10.1088/0004-637X/774/2/141
- Gonzalez, W., & Parker, E. 2016, Magnetic Reconnection, Vol. 427, doi: 10.1007/978-3-319-26432-5
- Gopalswamy, N. 2003, Advances in Space Research, 31, 869, doi: 10.1016/S0273-1177(02)00888-8
- Gosling, J. T., Borrini, G., Asbridge, J. R., et al. 1981, J. Geophys. Res., 86, 5438, doi: 10.1029/JA086iA07p05438
- Guo, W. P., & Wu, S. T. 1998, ApJ, 494, 419, doi: 10.1086/305196
- Guo, W. P., Wu, S. T., & Tandberg-Hanssen, E. 1996, ApJ, 469, 944, doi: 10.1086/177841
- Hodgson, J. D. B., & Neukirch, T. 2015, Geophysical and Astrophysical Fluid Dynamics, 109, 524,
 - doi: 10.1080/03091929.2015.1081188
- Hsieh, M.-S., & Otto, A. 2015, J. Geophys. Res., 120, 4264, doi: 10.1002/2014JA020925
- Jackman, C. M., Arridge, C. S., André, N., et al. 2014, SSRv, 182, 85,
 - doi: 10.1007/s11214-014-0060-8
- Kivelson, M. G., McPherron, R. L., Thompson, S., et al. 2005, Advances in Space Research, 36, 1818, doi: 10.1016/j.asr.2004.03.024
- Korreck, K. E., Szabo, A., Nieves Chinchilla, T., et al. 2020, ApJS, 246, 69, doi: 10.3847/1538-4365/ab6ff9
- Lapenta, G., & Knoll, D. A. 2003, SoPh, 214, 107, doi: 10.1023/A:1024036917505

- Lee, J.-O., Cho, K.-S., An, J., et al. 2021, ApJL, 920, L6, doi: 10.3847/2041-8213/ac2422
- Liewer, P. C., Qiu, J., Vourlidas, A., Hall, J. R., & Penteado, P. 2021, A&A, 650, A32, doi: 10.1051/0004-6361/202039641
- Lin, Y., Wang, X. Y., Lu, S., Perez, J. D., & Lu,Q. 2014, J. Geophys. Res., 119, 7413,doi: 10.1002/2014JA020005
- Lin, Y., Wing, S., Johnson, J. R., et al. 2017,Geophys. Res. Lett., 44, 5892,doi: 10.1002/2017GL073957
- Linker, J. A., Lionello, R., Mikić, Z., & Amari, T. 2001, J. Geophys. Res., 106, 25165, doi: 10.1029/2000JA004020
- Liu, Y.-H., Birn, J., Daughton, W., Hesse, M., & Schindler, K. 2014, J. Geophys. Res., 119, 9773, doi: 10.1002/2014JA020492
- Lu, S., Artemyev, A. V., Angelopoulos, V., Lin, Y., & Wang, X. Y. 2017, J. Geophys. Res., 122, 8295, doi: 10.1002/2017JA024209
- Lu, S., Lin, Y., Angelopoulos, V., et al. 2016,J. Geophys. Res., 121, 11,doi: 10.1002/2016JA023325
- Lu, S., Artemyev, A. V., Angelopoulos, V., et al. 2019, Journal of Geophysical Research (Space Physics), 124, 1052, doi: 10.1029/2018JA026202
- McFadden, J. P., Carlson, C. W., Larson, D., et al. 2008, SSRv, 141, 277, doi: 10.1007/s11214-008-9440-2
- Mignone, A., Bodo, G., Massaglia, S., et al. 2007, ApJS, 170, 228, doi: 10.1086/513316
- Nakamura, R., Baumjohann, W., Klecker, B., et al. 2002, Geophys. Res. Lett., 29, 200000, doi: 10.1029/2002GL015763
- Nakamura, R., Retinò, A., Baumjohann, W., et al. 2009, Annales Geophysicae, 27, 1743
- Neukirch, T. 1995a, A&A, 301, 628
- —. 1995b, Physics of Plasmas, 2, 4389, doi: 10.1063/1.870995
- —. 1997, A&A, 325, 847
- Nickeler, D. H., & Wiegelmann, T. 2010, Annales Geophysicae, 28, 1523,
 - doi: 10.5194/angeo-28-1523-2010
- Nieves-Chinchilla, T., Szabo, A., Korreck, K. E., et al. 2020, ApJS, 246, 63, doi: 10.3847/1538-4365/ab61f5
- Nishimura, Y., & Lyons, L. R. 2016, Journal of Geophysical Research (Space Physics), 121, 1327, doi: 10.1002/2015JA022128

- Ofman, L., Abbo, L., & Giordano, S. 2011, ApJ, 734, 30, doi: 10.1088/0004-637X/734/1/30
- Ofman, L., Provornikova, E., Abbo, L., & Giordano, S. 2015, Annales Geophysicae, 33, 47, doi: 10.5194/angeo-33-47-2015
- Parker, E. N. 1994, Spontaneous current sheets in magnetic fields: with applications to stellar x-rays. International Series in Astronomy and Astrophysics, Vol. 1. New York: Oxford University Press, 1994., 1
- Petrukovich, A. A., Artemyev, A. V., Nakamura, R., Panov, E. V., & Baumjohann, W. 2013, J. Geophys. Res., 118, 5720, doi: 10.1002/jgra.50550
- Petrukovich, A. A., Artemyev, A. V., Vasko, I. Y., Nakamura, R., & Zelenyi, L. M. 2015, SSRv, 188, 311, doi: 10.1007/s11214-014-0126-7
- Petrukovich, A. A., Baumjohann, W., Nakamura, R., & Rème, H. 2009, J. Geophys. Res., 114, 9203, doi: 10.1029/2009JA014064
- Petrukovich, A. A., Baumjohann, W., Nakamura,R., et al. 2007, J. Geophys. Res., 112, 10213,doi: 10.1029/2007JA012349
- Petrukovich, A. A., Mukai, T., Kokubun, S., et al. 1999, J. Geophys. Res., 104, 4501, doi: 10.1029/98JA02418
- Pneuman, G. W. 1972, SoPh, 23, 223, doi: 10.1007/BF00153906
- Pneuman, G. W., & Kopp, R. A. 1971, SoPh, 18, 258, doi: 10.1007/BF00145940
- Priest, E. 2016, in Astrophysics and Space Science Library, Vol. 427, Astrophysics and Space Science Library, ed. W. Gonzalez & E. Parker, 101, doi: 10.1007/978-3-319-26432-5-3
- Priest, E. R. 1985, Reports on Progress in Physics, 48, 955, doi: 10.1088/0034-4885/48/7/002
- Priest, E. R., & Forbes, T. G. 2002, A&A Rv, 10, 313, doi: 10.1007/s001590100013
- Pritchett, P. L., & Coroniti, F. V. 1994,Geophys. Res. Lett., 21, 1587,doi: 10.1029/94GL01364
- —. 1995, J. Geophys. Res., 100, 23551, doi: 10.1029/95JA02540
- Pritchett, P. L., & Lu, S. 2018, J. Geophys. Res., 123, 2787, doi: 10.1002/2017JA025094
- Rastätter, L., Hesse, M., & Schindler, K. 1999,J. Geophys. Res., 104, 12301,doi: 10.1029/1999JA900138

- Reeves, K. K., Guild, T. B., Hughes, W. J., et al. 2008, J. Geophys. Res., 113, 0, doi: 10.1029/2008JA013049
- Réville, V., Velli, M., Rouillard, A. P., et al. 2020a, ApJL, 895, L20, doi: 10.3847/2041-8213/ab911d
- Réville, V., Velli, M., Panasenco, O., et al. 2020b, ApJS, 246, 24,
 - doi: 10.3847/1538-4365/ab4fef
- Réville, V., Fargette, N., Rouillard, A. P., et al. 2021, arXiv e-prints, arXiv:2112.07445. https://arxiv.org/abs/2112.07445
- Rich, F. J., Vasyliunas, V. M., & Wolf, R. A. 1972, J. Geophys. Res., 77, 4670,doi: 10.1029/JA077i025p04670
- Runov, A., Angelopoulos, V., Artemyev, A. V., et al. 2021a, Journal of Atmospheric and Solar-Terrestrial Physics, 220, 105671, doi: 10.1016/j.jastp.2021.105671
- Runov, A., Sergeev, V. A., Nakamura, R., et al. 2005, Planet. Space Sci., 53, 237, doi: 10.1016/j.pss.2004.09.049
- —. 2006, Annales Geophysicae, 24, 247
- Runov, A., Angelopoulos, V., Sitnov, M. I., et al. 2009, Geophys. Res. Lett., 36, L14106, doi: 10.1029/2009GL038980
- Runov, A., Grandin, M., Palmroth, M., et al. 2021b, Annales Geophysicae, 39, 599, doi: 10.5194/angeo-39-599-2021
- Schindler, K., & Birn, J. 1978, PhR, 47, 109, doi: 10.1016/0370-1573(78)90016-9
- —. 1986, Space Science Reviews, 44, 307,
 doi: 10.1007/BF00200819
- —. 1999, J. Geophys. Res., 104, 25001, doi: 10.1029/1999JA900258
- Schindler, K., Birn, J., & Janicke, L. 1983, SoPh, 87, 103, doi: 10.1007/BF00151164
- Shi, C., Artemyev, A., Velli, M., & Tenerani, A. 2021, Journal of Geophysical Research (Space Physics), 126, e29711, doi: 10.1029/2021JA029711
- Sitnov, M. I., Swisdak, M., & Divin, A. V. 2009,J. Geophys. Res., 114, A04202,doi: 10.1029/2008JA013980
- Sitnov, M. I., Birn, J., Ferdousi, B., et al. 2019, SSRv, 215, 31, doi: 10.1007/s11214-019-0599-5
- Snekvik, K., Tanskanen, E., Østgaard, N., et al.
 2012, J. Geophys. Res., 117, 2219,
 doi: 10.1029/2011JA017040

- Steinhauer, L. C., McCarthy, M. P., & Whipple,E. C. 2008, J. Geophys. Res., 113, 4207,doi: 10.1029/2007JA012578
- Steinolfson, R. S., Suess, S. T., & Wu, S. T. 1982, ApJ, 255, 730, doi: 10.1086/159872
- Sun, W. J., Fu, S. Y., Wei, Y., et al. 2017,J. Geophys. Res., 122, 12,212,doi: 10.1002/2017JA024603
- Syrovatskii, S. I. 1981, Annual review of astronomy and astrophysics, 19, 163,
 - doi: 10.1146/annurev.aa.19.090181.001115
- Terasawa, T., Shibata, K., & Scholer, M. 2000, Advances in Space Research, 26, 573, doi: 10.1016/S0273-1177(99)01087-X
- Verneta, A. I., Antonucci, E., & Marocchi, D. 1994, SSRv, 70, 299, doi: 10.1007/BF00777884
- Wang, X., & Bhattacharjee, A. 1999,J. Geophys. Res., 104, 7045,doi: 10.1029/1998JA900124
- Washimi, H., Yoshino, Y., & Ogino, T. 1987, Geophys. Res. Lett., 14, 487, doi: 10.1029/GL014i005p00487
- Wiegelmann, T., & Schindler, K. 1995,Geophys. Res. Lett., 22, 2057,doi: 10.1029/95GL01980

- Woo, R. 1997, Geophys. Res. Lett., 24, 97, doi: 10.1029/96GL03479
- Wu, S. T., & Guo, W. P. 1997a, Advances in Space Research, 20, 2313, doi: 10.1016/S0273-1177(97)00902-2
- —. 1997b, Washington DC American Geophysical Union Geophysical Monograph Series, 99, 83, doi: 10.1029/GM099p0083
- Yeh, T. 1984, Ap&SS, 98, 353, doi: 10.1007/BF00651414
- Yeh, T., & Pneuman, G. W. 1977, SoPh, 54, 419, doi: 10.1007/BF00159933
- Yin, L., & Winske, D. 2002, Journal of Geophysical Research (Space Physics), 107, 1485, doi: 10.1029/2002JA009507
- Yushkov, E., Petrukovich, A., Artemyev, A., & Nakamura, R. 2021, Journal of Geophysical Research: Space Physics, 126, e2020JA028969, doi: https://doi.org/10.1029/2020JA028969
- Zaharia, S., Birn, J., & Cheng, C. Z. 2005,J. Geophys. Res., 110, A09228,doi: 10.1029/2005JA011101
- Zharkova, V. V., Arzner, K., Benz, A. O., et al. 2011, SSRv, 159, 357, doi: 10.1007/s11214-011-9803-y